Impact sound insulation prediction with a modal transfer matrix method and a detailed source model

J. Vastiau, C. Van hoorickx, E.P.B. Reynders
KU Leuven, Department of Civil Engineering,
Kasteelpark Arenberg 40, box 2448, B-3001, Leuven, Belgium

Abstract
The modal Transfer Matrix Method (mTMM) has recently been developed to predict the impact sound radiation from layered floors resulting from tapping machine impacts, while accounting for simply supported boundary conditions. In this work, a detailed source model is presented which accounts for both the impact locations of the individual hammers and the discrete 2 Hz force spectrum. It is also discussed how this detailed source model can be implemented into the mTMM. Monte Carlo simulations provide insight into the uncertainty of the radiated sound power from bare and layered floors, resulting from the impact force location. Narrow-band sound pressure level measurements on a layered floor have been performed to validate the detailed source model and its use in the mTMM. A comparison of measured and predicted results indicates the importance of such a detailed source approach at low frequencies, since measurement results display peaks at discrete 2 Hz values which cannot be predicted using a simplified source model.

1 Introduction

Detailed measurements of the acceleration level of a timber joist floor have indicated a 2 Hz line spectrum for the ISO tapping machine [1], while it is commonly assumed that a single hammer impacts the floor with a base frequency of 10 Hz [2]. These measurements also indicated that in general, there is a difference in amplitude of about 20 dB between the 10 Hz lines and the 2 Hz lines, meaning that the 10 Hz lines are usually the most important ones in the impact spectrum. However, the 2 Hz lines can become important, especially at low frequencies and for lightweight floors. A recent measurement campaign has demonstrated that such a 2 Hz line spectrum and a 20 dB difference between the 10 Hz lines and the 2 Hz lines is also present in narrow-band spectra of the sound pressure level in the receiver room [3].

In this work, a detailed source model is presented which accounts for the exact impact locations of the tapping machine hammers. The mathematical formulation is also derived on how this detailed source model can be implemented into the recently developed mTMM [4, 5, 6]. The presented method now accounts for both the modal behaviour of the structure, resulting from the boundary conditions, and the 2 Hz line spectrum, resulting from the detailed source model. The extended method is computationally efficient and is used in Monte Carlo simulations to determine the uncertainty related to the positioning of the tapping machine. These Monte Carlo simulations are also used to indicate how averaging the results over multiple tapping machine positions can significantly reduce the uncertainty with respect to a single tapping machine position.

The extended mTMM is validated in two steps: first, a numerical validation is performed by comparing the mTMM to two finite element (FE) models for the sound pressure level and the impact sound insulation improvement of bare and layered floors. Two FE models are considered to investigate the influence of adjoining concrete slabs which are rigidly connected to the test element. Second, the mTMM is experimentally validated using narrow-band measurements, which confirm the need for a detailed source model at low frequencies.

This work is organized as follows: the detailed source model is presented in section 2, as well as the implementation of this source model into the mTMM framework. In section 3, the mTMM is validated numerically using two FE models. In section 4, the uncertainty on impact sound radiation related to the tapping machine

positioning is discussed. Experimental validation is included in section 5, using narrow-band measurements of the sound pressure level in the receiver room as a result of tapping machine impacts. Section 6 contains the conclusions.

2 Use of a detailed source model in the mTMM

First, the impact forces of all tapping machine hammers are derived, assuming that all hammers impact at the same location. The phase differences between these forces then determine whether or not one single discrete frequency component is excited. Second, a force-pressure load relation is derived for these impact sources, accounting for the different positions at which the hammers impact the floor. This relation ensures that the detailed source model is compatible with the mTMM, which uses a generalized pressure load as an excitation source.

2.1 Detailed source model

If excitation of the structure is harmonic at frequency ω_0, then the impact force $F(t)$ can be expressed as

$$F(t) = |F|\mathrm{Re}(\mathrm{e}^{\mathrm{i}\omega_0 t}). \tag{1}$$

A tapping machine produces a periodic impact force, which can be represented by an exponential form of the Fourier series [2]:

$$F(t) = \sum_{n=-\infty}^{\infty} F_n \mathrm{Re}\left(\mathrm{e}^{\mathrm{i}n\omega_0 t}\right) \tag{2}$$

with $\omega_0 = \frac{2\pi}{T}$, $F_n = \frac{1}{T}\int_0^T F(t)\mathrm{Re}\left(\mathrm{e}^{\mathrm{i}n\omega_0 t}\right)\mathrm{d}t$.

where F_n represents the amplitude of the n^{th} harmonic component. For a standard tapping machine, each hammer has a mass of m = 0.5 kg and a free-drop height of h = 0.04 m, as specified by ISO 10140-5:2010 [7]. The hammers impact the floor surface at a rate of 10 times per second, leading to a fundamental frequency of f_0 = 10 Hz or a period of T = 0.1 s. When exciting a stiff and heavy structure with tapping machine hammers, $\mathrm{e}^{\mathrm{i}n\omega_0 t} \approx 1$ [2] because the striking of the hammer causes a force impulse duration which is small compared to even the highest period of interest when exciting massive structures such as concrete slabs. The impulse-momentum theorem [8] is used to express the force in terms of the known mass and drop height of the hammers, assuming ideal elastic impacts to obtain an upper limit for the force amplitude [1]. Fig. 1 shows the time history of impact force $F(t)$ and its Fourier series coefficients F_n, which are expressed as

$$F_n \approx \frac{1}{T}\int_0^T F(t)\mathrm{d}t = \frac{2mv_0}{T} = \frac{2m}{T}\sqrt{2gh} = 8.86\,\mathrm{N}. \tag{3}$$

Alternatively, all five impact hammers and their respective locations can be accounted for, yielding a more accurate prediction of the actual impact forces of the tapping machine, hence the term ‘detailed’ source model. Considering the contribution of each impact hammer separately, the period of a single hammer equals $T = 0.5\,\mathrm{s}$ and the time delay between consecutive impacts of two different hammers is $0.1\,\mathrm{s}$. The Fourier series coefficients for hammer 1 are obtained in the same way as Eq. (3):

$$F_n^{(1)} \approx \frac{1}{T}\int_0^T F^{(1)}(t)\mathrm{d}t = \frac{2mv_0}{T} = \frac{2m}{T}\sqrt{2gh} = 1.77\,\mathrm{N}. \tag{4}$$

The order of impacts from the hammers is 1-3-5-2-4, with an interval of 0.1 s between each hammer. The

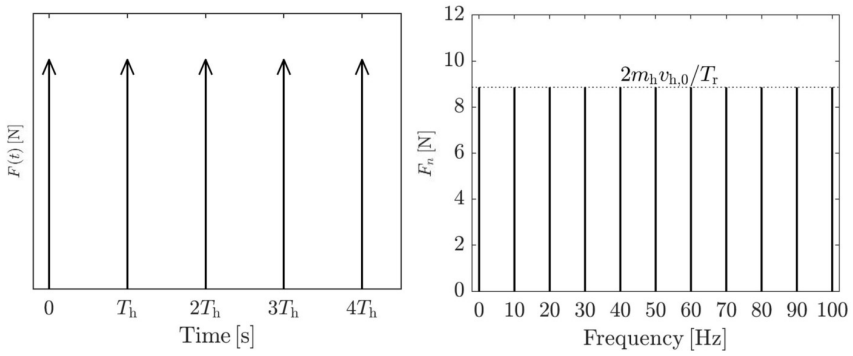

(a) (b)

Figure 1: (a) The harmonic impact force and (b) its Fouries series coefficients [9].

time signal of the $\mathrm{k^{th}}$ hammer displays a delay t_k with respect to the first hammer at t = 0 s, so:

$$F^{(k)}(t-t_k) = \sum_{n=-\infty}^{\infty} F_n^{(k)} \mathrm{Re}\left(e^{\mathrm{i}\frac{2\pi n}{T}(t-t_k)}\right). \tag{5}$$

This constitutes a phase angle $-\frac{2\pi n}{T}t_k$ for the $\mathrm{n^{th}}$ harmonic of hammer k. The phase angles of all hammers are visualized in Fig. 2, showing that the forces always cancel each other out, except at multiple frequencies of 10 Hz where all hammers act in phase. Of course this conclusion only holds under the assumption that all hammers hit the structure at the exact same location. If the differences in impact location are accounted for, the force amplitudes will vary due to the fact that the floor has a location-dependent point mobility, such that the phases will no longer cancel the hammer forces out entirely and sound radiation at multiple frequencies of 2 Hz can occur.

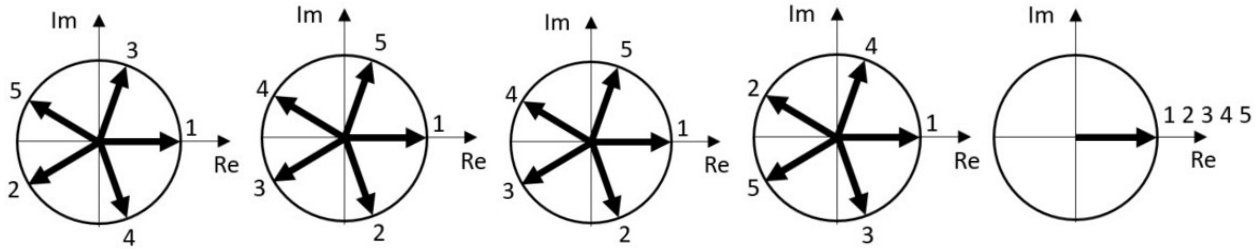

(a) (b) (c) (d) (e)

Figure 2: Phase angle for each of the five hammers (a) 1^{st} harmonic (2 Hz), (b) 2^{nd} harmonic (4 Hz), (c) 3^{rd} harmonic (6 Hz), (d) 4^{th} harmonic (8 Hz) and (e) 5^{th} harmonic (10 Hz).

2.2 A generalized force-pressure relation for compatibility of the detailed source model and mTMM

We will now derive a relation between the external force F and the generalized pressure load p_j on a plate, excited by a vertical point force at an arbitrary position $(x_\mathrm{f}, y_\mathrm{f})$. The vertical impact force is related to the normal pressure load exerted by the hammer onto the floor surface by integration of this pressure load over the floor surface area. The relation between force and pressure load is used in the mTMM to apply the point force as an external normal pressure load on the floor boundary. The pressure load in the frequency domain is obtained from a summation of the Fourier series coefficients of the point force:

$$p(x,y,\omega) = F(\omega)\delta(x-x_\mathrm{f})\delta(y-y_\mathrm{f}) \tag{6}$$

where $\delta(x - x_\mathrm{f})$ is the Dirac delta function and the force $F(\omega)$ is the Fourier transform of the time history of the force signal $F(t)$.

The mTMM approximates the velocity field using a Ritz approach, i.e. by means of a generalized velocity $v_j(z,\omega)$ and a finite set of shape functions $\phi_j(x,y)$ that satisfy the boundary conditions at any coordinate z. The shape functions are expected to approximate the mode shapes of the floor. It has been derived in previous work that this decomposition also holds for the pressure load on the floor boundary [4]:

$$v(x,y,z,\omega) = \sum_{j=1}^{N_m} v_j(z,\omega)\phi_j(x,y), \qquad p(x,y,\omega) = \sum_{j=1}^{N_m} p_j(\omega)\phi_j(x,y). \tag{7}$$

Scaled sine functions have been chosen as shape functions [10]:

$$\phi_j(x,y) = \frac{2}{\sqrt{\rho t L_\mathrm{x} L_\mathrm{y}}} \sin\left(k_{jx}x\right)\sin\left(k_{jy}y\right) \quad \text{where } k_{jx} = \frac{m_j\pi}{L_\mathrm{x}} \text{ and } k_{jy} = \frac{n_j\pi}{L_\mathrm{y}}, \tag{8}$$

ρ is the mass density, t is the floor thickness and m_j and n_j are the number of half wavelengths in the x and y-directions, respectively.

The shape functions $\phi_j(x,y)$ are orthogonal to each other, so the following equation is valid:

$$\begin{aligned}\int_0^{L_\mathrm{x}}\int_0^{L_\mathrm{y}} \phi_j(x,y)\phi_l(x,y)\mathrm{d}x\mathrm{d}y &= \int_0^{L_\mathrm{x}}\int_0^{L_\mathrm{y}} \frac{4}{\rho t L_\mathrm{x} L_\mathrm{y}} \sin^2\left(k_{jx}x\right)\sin^2\left(k_{jy}y\right)\delta_{jl}\,\mathrm{d}x\mathrm{d}y \\ &= \frac{4}{\rho t L_\mathrm{x} L_\mathrm{y}}\left(\frac{L_\mathrm{x}}{4}\left(2 - \frac{\sin(2m_j\pi)}{m_j\pi}\right)\right)\left(\frac{L_\mathrm{y}}{4}\left(2 - \frac{\sin(2n_j\pi)}{n_j\pi}\right)\right)\delta_{jl} \\ &= \frac{1}{\rho \mathrm{t}}\delta_{jl}\end{aligned} \tag{9}$$

where δ_{jl} is the Kronecker delta. To determine the generalized pressure load p_j at the impact side, an expression is required to relate the generalized pressure load to the impact force $F(\omega)$. The following equation employs the pressure load decomposition from Eq. (7):

$$\int_0^{L_\mathrm{x}}\int_0^{L_\mathrm{y}} \phi_j(x,y)p(x,y,\omega)\mathrm{d}x\mathrm{d}y = \sum_{l=1}^{N_m}\int_0^{L_\mathrm{x}}\int_0^{L_\mathrm{y}} \phi_j(x,y)\phi_l(x,y)p_l(\omega)\mathrm{d}x\mathrm{d}y. \tag{10}$$

Using the orthogonality property from Eq. (9) results in

$$\int_0^{L_\mathrm{x}}\int_0^{L_\mathrm{y}} \phi_j(x,y)p(x,y,\omega)\mathrm{d}x\mathrm{d}y = \frac{1}{\rho t}p_j(\omega) \tag{11}$$

and subsequent substitution of this force-pressure relation into Eq. (6) and evaluation of the integral yields a relation between the generalized pressure load and the impact force:

$$p_j(\omega) = \rho \mathrm{t}\phi_j(x_\mathrm{f}, y_\mathrm{f})F(\omega). \tag{12}$$

3 Numerical validation of the mTMM with a detailed source model

In the previous section, a detailed source model is presented, and a relation between the impact force and the generalized pressure load is derived such that the detailed source model can be implemented into the mTMM. In this section, a floating floor with horizontal dimensions $L_\mathrm{x} = 2.6\,\mathrm{m}$ and $L_\mathrm{y} = 4.4\,\mathrm{m}$ is assessed numerically, using both the mTMM and a finite element (FE) model. Both methods predict the sound power level radiated into the receiver room by the mechanically excited floating floor and the impact sound insulation improvement of layered floors with respect to a reference concrete base floor. Two cases have been

studied next to the concrete base floor: case 1 is a three-layer floor, consisting of the concrete base floor, a thermal insulation layer (cement-based mortar with fine EPS beads) and a finishing screed. Case 2 is a four-layer floor with an added acoustic interlayer (PE-foam) between the thermal insulation and the finishing screed. The mechanical properties of all layers have been experimentally determined by the Belgian Building Research Institute (BBRI) [11] and are listed in Table 1, with the layer thickness t, mass density ρ, damping ratio η, Poisson coefficient ν and the modulus of elasticity E.

Table 1: Mechanical properties for all layers of the different cases.

	$t[\mathrm{m}]$	$\rho[\frac{\mathrm{kg}}{\mathrm{m}^3}]$	η [-]	ν [-]	$E[\frac{\mathrm{N}}{\mathrm{m}^2}]$
Finishing screed	0.06	1900	0.015	0.2	$17.4 \cdot 10^9$
Acoustic interlayer	0.008	25	0.3	0.2	$2.4 \cdot 10^5$
Thermal layer	0.065	125	0.1	0.2	$1.8 \cdot 10^7$
Concrete base floor	0.14	2445	0.015	0.2	$22 \cdot 10^9$

The 14 cm thick concrete base floor (test element: horizontal dimensions $L_\mathrm{x} = 4.4\,\mathrm{m}$ and $L_\mathrm{y} = 2.6\,\mathrm{m}$) is rigidly connected to a 30 cm thick concrete frame, which is 25 cm wide in both horizontal directions. This frame also has rigid connections to the adjoining concrete slabs of 30 cm thickness through a cemented joint. The entirety of the test element, frame and adjoining slabs will be called the full structure, which has plane dimensions $L_\mathrm{x} = 4.90\,\mathrm{m}$ and $L_\mathrm{y} = 6.30\,\mathrm{m}$. This full structure (cfr. Fig. 3 (b)) is decoupled from adjacent floors by means of air gaps, filled with mineral wool. The full structure is implemented in the FE model (cfr. Fig. 3 (a)), whereas the mTMM includes only the test element since this method can only account for homogeneous layers. In order to investigate the influence of the adjoining concrete slabs, a second FE model, including only the test element, is produced.

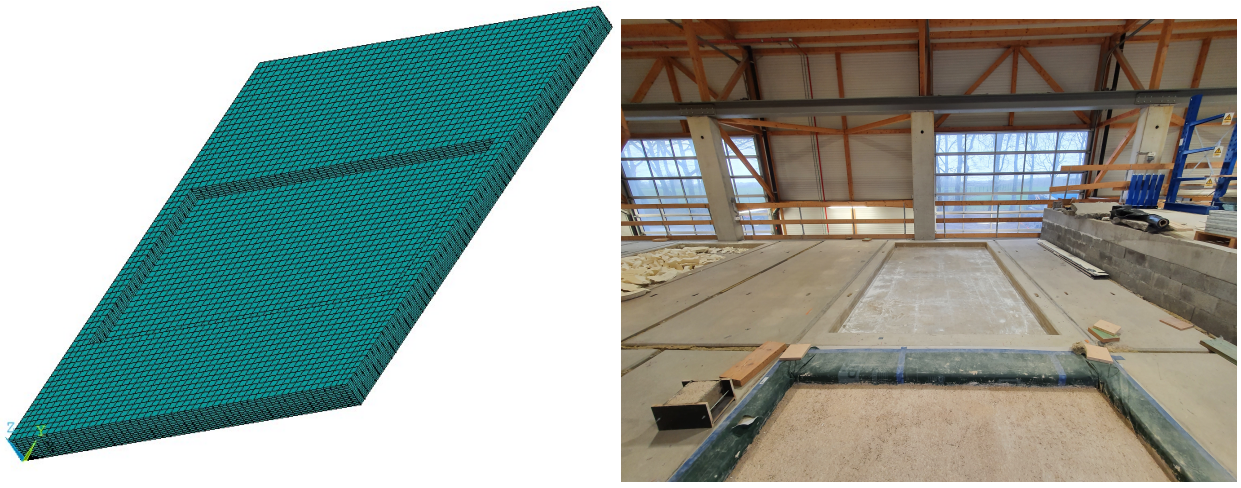

(a) (b)

Figure 3: Full structure, including the test element and the adjoining thick, concrete slabs: (a) FE model of the full structure and (b) laboratory setup.

The mTMM predictions for the sound pressure level for all cases, resulting from hammer impacts at the middle of the floor $\mathrm{x_f} = 2.2\,\mathrm{m}$ and $\mathrm{y_f} = 1.3\,\mathrm{m}$ and an orientation of the tapping machine parallel to the x-axis, are compared to both FE models in Fig. 4. The base floor displays clear modes in the one-third octave bands centered at 40 Hz, 125 Hz and 250 Hz, all of which are not present or less pronounced in the FE model of the full structure. The simplified FE model, however, which only includes the test element, contains a very similar behavior at these frequencies. There is an overall good agreement between the mTMM and the simplified FE model, and both predictions are significantly different from the FE model of the full structure. The adjoining concrete slabs significantly change the resonance frequencies of the structure, which influences the prediction results at low frequencies. At high frequencies, the presence of the adjoining slabs results in lower predictions with respect to the mTMM and the simplified FE model since the main purpose of these

slabs is to provide additional edge damping to the test element. The same conclusions hold for case 1, where the low-frequent modes are similar for the mTMM and the simplified FE model, whereas the full FE model deviates at low frequencies due to the altered resonance frequencies. For cases 1 and 2 a good agreement between all three models is observed when the different layers decouple (i.e. above the mass-spring-mass resonance frequency).

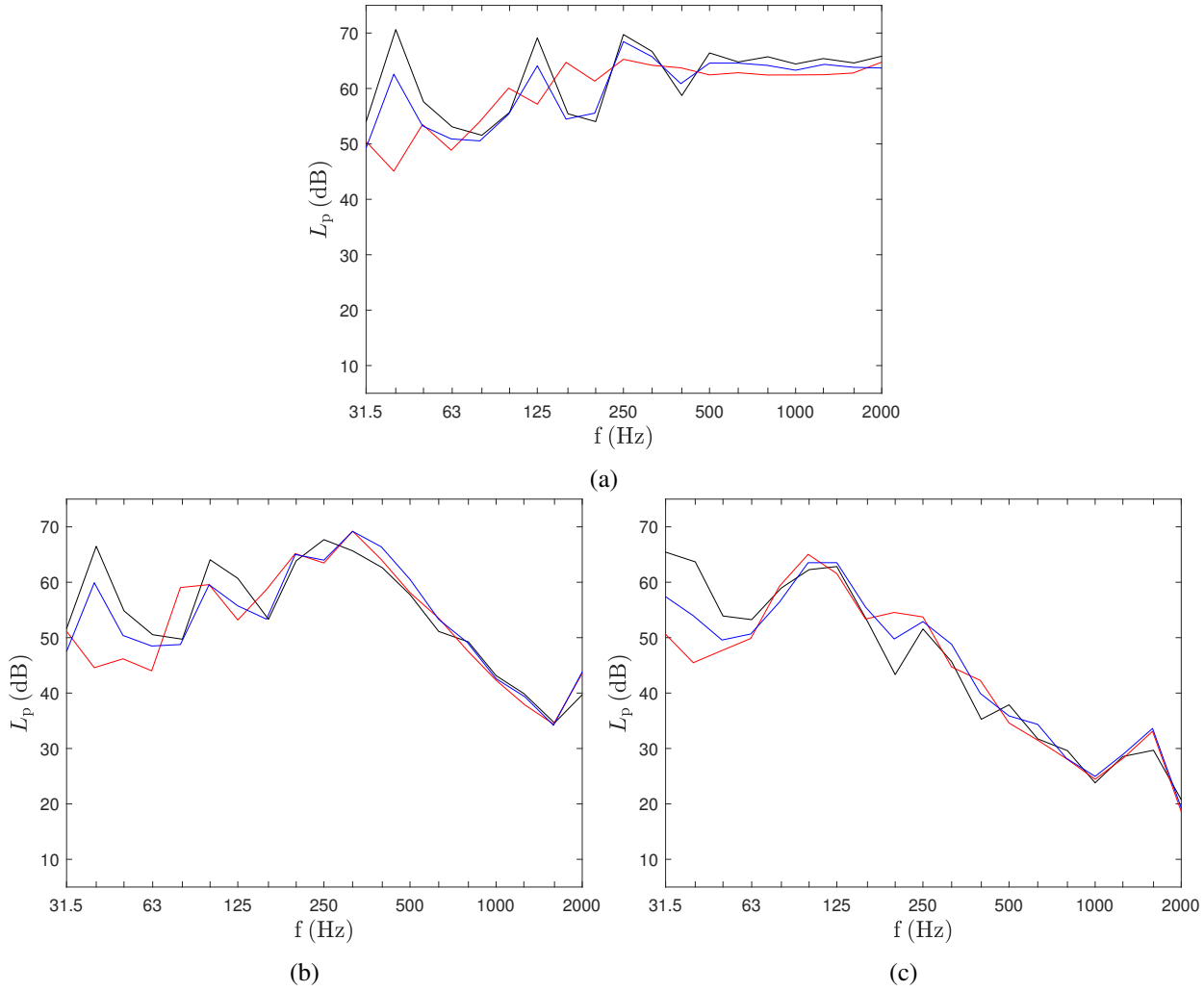

Figure 4: Numerical prediction of the impact sound pressure level in the receiver room. The mTMM is displayed in black, the full FE prediction in red and the FE prediction of the test element only in blue: (a) base concrete floor, (b) case 1, (c) case 2.

Comparing the impact sound insulation improvement from the mTMM and the FE models, an overall good agreement can be observed from Fig. 5, following the good agreement between the predicted sound pressure levels. It is observed that the simplified FE model and the mTMM prediction are similar, whereas the full FE model deviates at low frequencies due to the altered resonance frequencies resulting from the adjoining concrete slabs.

The FE and mTMM methods can also be compared in terms of computational efficiency. For a frequency range including the one-third octave bands from 31.5 Hz to 2000 Hz, the FE model of case 1 takes a total time of approximately 7 hours and 7 minutes to run, while the computational cost of the mTMM only amounts to 6 seconds, which means that the proposed approach runs approximately 4270 times faster than the FE model. If the entire building acoustics frequency range up to 5000 Hz would be included in the comparison, the relative difference would become even larger, with the FE model needing finer mesh sizes.

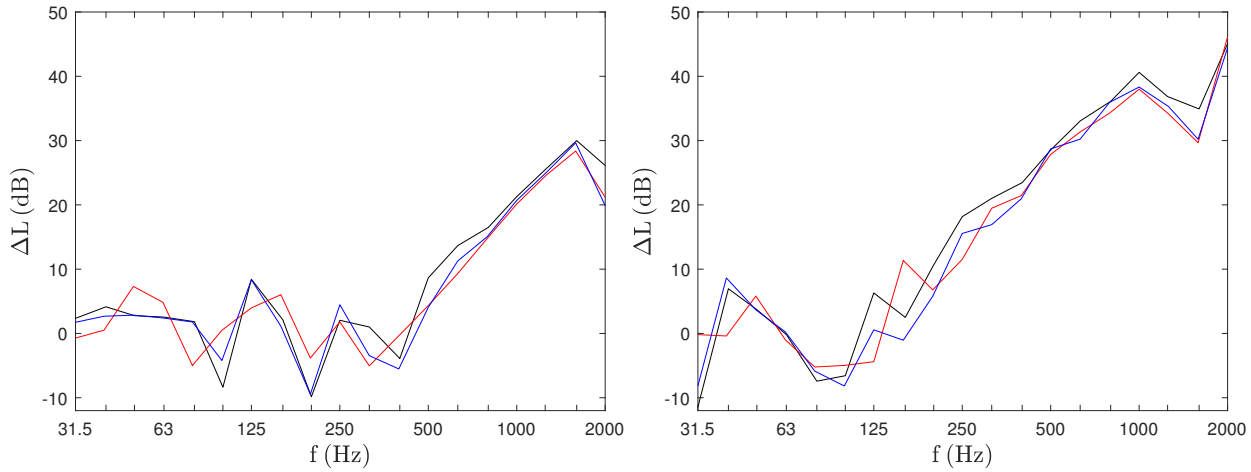

Figure 5: Numerical prediction of the impact sound insulation improvement of layered floors. The mTMM is displayed in black, the full FE prediction in red and the FE prediction of the test element only in blue. (a) Case 1, (b) case 2.

4 Uncertainty on impact sound radiation related to tapping machine positions

In the previous section, a numerical validation of the mTMM is provided. In this section, the uncertainty of mTMM predictions related to tapping machine positions is reported. The uncertainty is quantified for two specific variables: the sound pressure level L_p and the impact sound insulation improvement ΔL. For both variables, the uncertainty is quantified in two ways: first, the impact force is moved systematically across the test element to find the maximum variation that can occur from a single tapping machine position. The uncertainty is quantified by the 95 % confidence interval. Second, a Monte Carlo simulation is performed with 1000 samples. For each sample, five tapping machine positions were selected, spaced at least 0.5 m from the edge and 0.7 m from other tapping machine positions in accordance to ISO 10140-3 [12]. The variable of interest (L_p or ΔL) is obtained for each individual sample as an average over the quadratic sound pressures of the five tapping machine positions [12]. The mean value is finally obtained by averaging L_p or ΔL over all samples. Fig. 6 illustrates the mean value and 95 % confidence interval for both cases, as well as the concrete base floor and shows that the uncertainty on the single position is much larger than the uncertainty on five positions, as is to be expected.

The uncertainty is low if there are no modes in a one-third octave band, for example at 100 Hz for the concrete base floor. However, the uncertainty is largest when just a single mode is present in a one-third octave band, for example at 80 Hz for the concrete base floor, at 125 Hz for case 1 or at 63 and 100 Hz for case 2. In case of a single mode, the impact sound radiation depends heavily on how well the impact force can excite the mode. If the force is located close to or exactly at a nodal point, the mode will respectively be excited weakly or not at all, whereas the sound pressure level in the receiver room is significantly higher if the force is located close to or at an antinode (location where the amplitude of the mode reaches a maximum value) of the mode.

In contrast to a single impact position, averaging over five positions yields more consistent results. Table 2 lists the width of the 95 % confidence intervals for both a single and five impact positions in the one-third octave band centered at 200 Hz. In general, the uncertainty is around 3-4 times lower in case of five impact positions (3.5 - 3.8 dB) with respect to the single impact position (11.6 - 12.4 dB). For both simulation types, the uncertainty tends to decrease with increasing frequency, as the modal overlap increases and therefore the probability of exciting multiple modes in the corresponding one-third octave band.

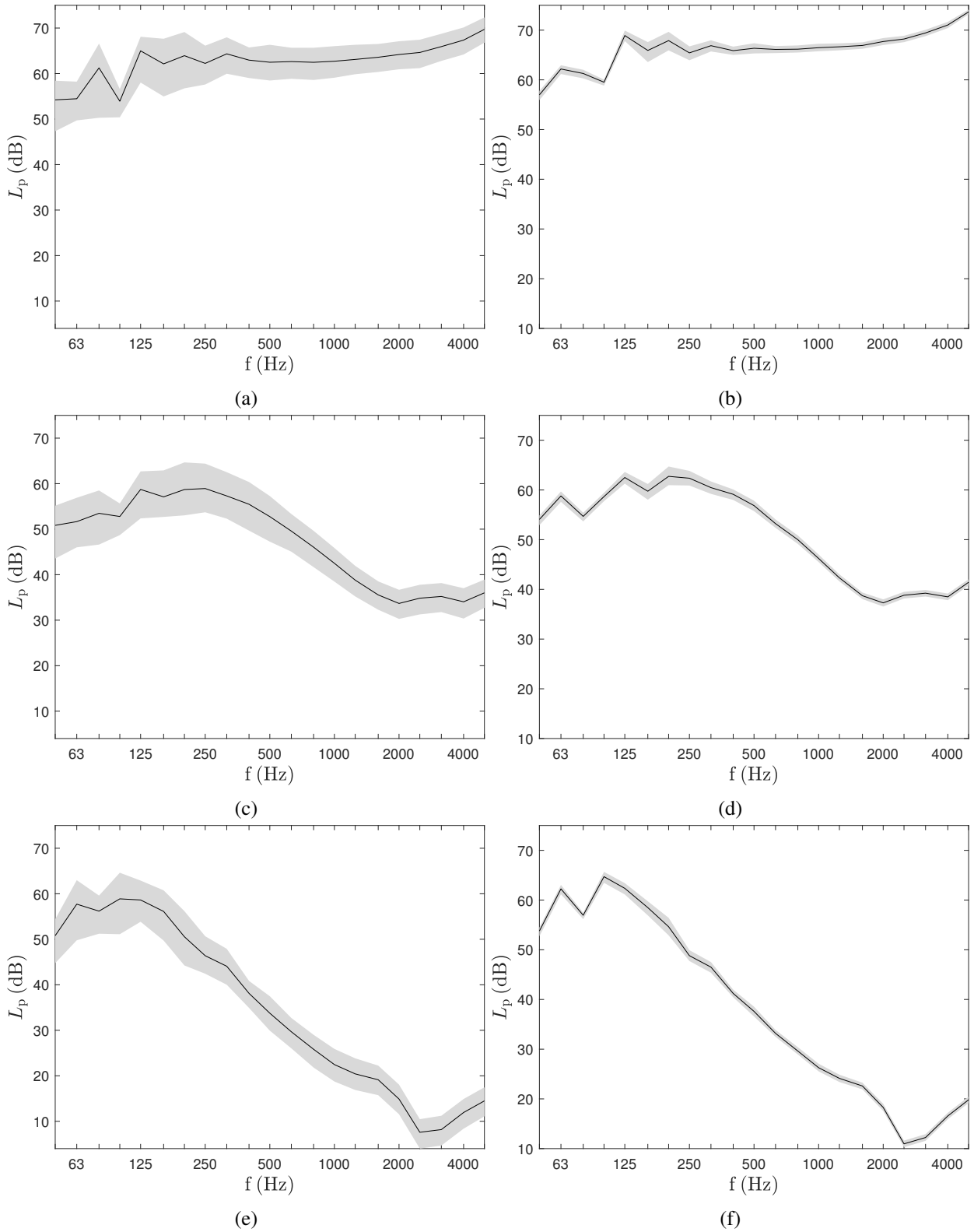

Figure 6: Mean and 95 % confidence interval for the predicted sound pressure level in the receiver room. (a)-(c)-(e) Variation of a single impact force position, (b)-(d)-(f) Monte Carlo simulation including five tapping machine positions per sample. (a)-(b) Concrete base floor, (c)-(d) case 1, (e)-(f) case 2.

The uncertainty on the single number rating of the standardized impact sound pressure level for the base floor and both cases 1 and 2 is also computed. The standardized impact sound pressure level is computed

Table 2: Width of the 95 % confidence intervals for the impact sound radiation in the one-third octave band centered at 200 Hz of various floors for a varying single tapping machine position and five tapping machine positions.

L_{p}	One impact position	Five impact positions
Base floor	12.4 dB	3.7 dB
Case 1	11.6 dB	3.8 dB
Case 2	11.9 dB	3.5 dB

according to NBN EN ISO 12354-2 [13]:

$$L_{\mathrm{nT}} = L_{\mathrm{p}} - 10 \log \left(\frac{T}{T_0} \right) \tag{13}$$

where $T_0 = 0.5\,\mathrm{s}$ is the reference reverberation time. The mean single numbers ratings amount to $63.3\ \mathrm{dB}$ for the base floor, $50.6\ \mathrm{dB}$ for case 1 and $30.3\ \mathrm{dB}$ for case 2. The width of the 95% confidence intervals is listed in Table 3, indicating that a reliable prediction of the single number rating is achieved with five tapping machine positions, whereas a single impact position yields an insufficiently accurate prediction of the single number rating for it to be used for design purposes.

Table 3: Width of the 95 % confidence intervals for the weighted standardized impact sound pressure level of various floors for a varying single tapping machine position and five tapping machine positions.

$L_{\mathrm{nT,w}}$	One impact position	Five impact positions
Base floor	4 dB	1 dB
Case 1	7 dB	1 dB
Case 2	6 dB	1 dB

The same conclusions hold for the impact sound insulation improvement of cases 1 and 2 with respect to the concrete base floor. A single impact force position yields much larger uncertainties (cfr. Table 4) than the five impact positions. The impact sound insulation improvement for both a single and five impact positions is displayed in Fig. 7, showing that the uncertainty on ΔL decreases more strongly with increasing frequency.

Table 4: 95 % confidence intervals for the impact sound insulation improvement in the one-third octave band centered at 200 Hz of both cases for a varying single tapping machine position and five tapping machine positions.

ΔL	One impact position	Five impact positions
Case 1	5.8 dB	1.4 dB
Case 2	3.4 dB	0.9 dB

5 Experimental validation of a layered floor

This section includes an experimental validation case for the mTMM framework. The test element now consists of the same four layers as decribed in the previous section, but with different layer thicknesses: the thermal insulation layer (cement mortar with EPS-beads) now has a thickness of 5 cm, and the lightweight concrete finishing screed also has a thickness of 5 cm. The mechanical properties of all layers have been measured by BBRI [11] and are listed in Table 5. These properties are used to perform a first, forward computation of the impact sound pressure level.

Impact forces are provided by a battery powered magnetic Tapping Machine Nor227. An overview of the tapping machine and the measured floor is displayed in Fig. 8. Three different tapping machine positions are

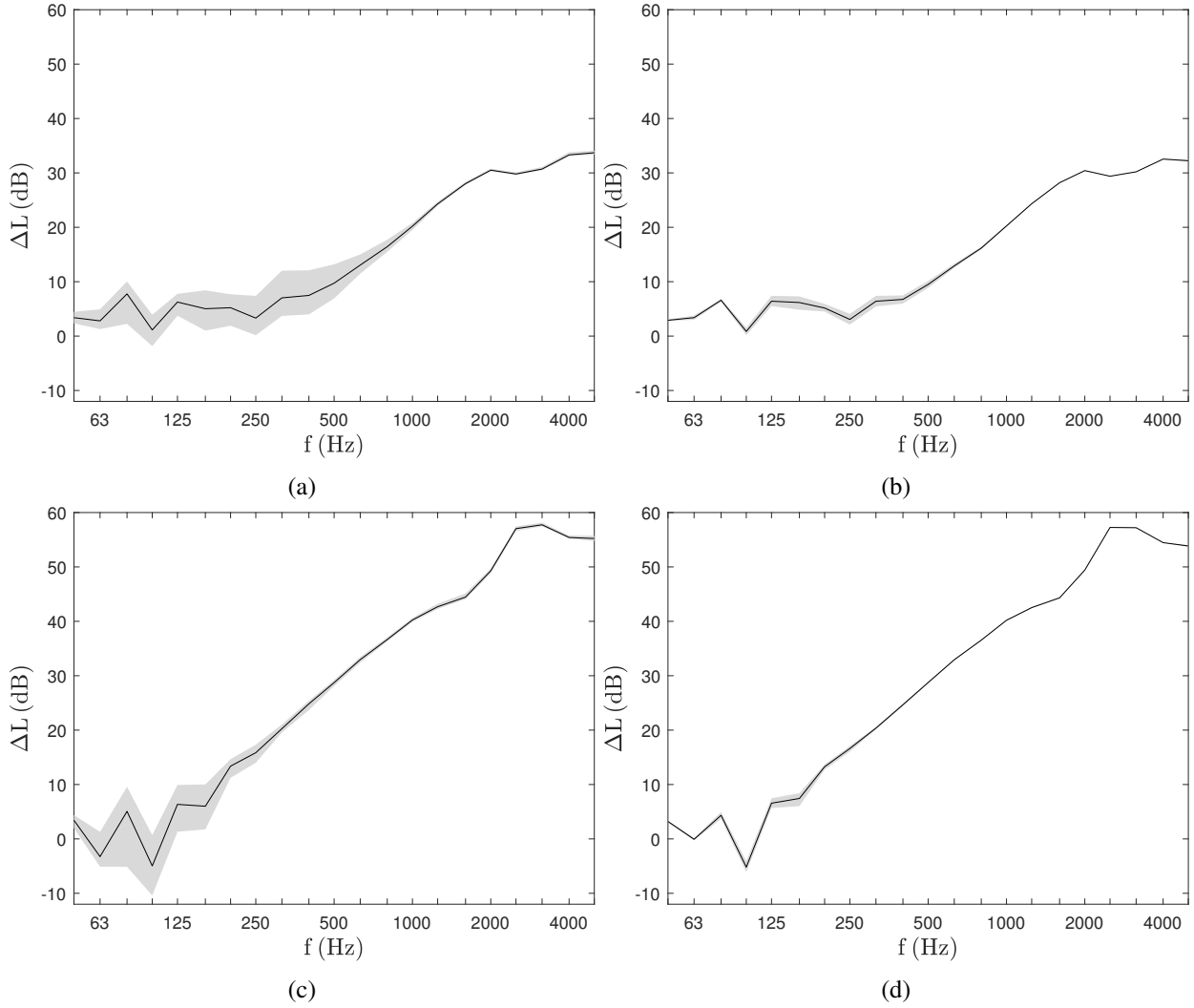

Figure 7: Mean and 95 % confidence interval for the predicted sound insulation improvement. (a)-(c) Variation of a single impact force position, (b)-(d) five tapping machine positions, (a)-(b) case 1, (c)-(d) case 2.

Table 5: Measured mechanical properties of each layer [11], used for forward computation of the sound pressure level. If a range of values is listed, the first value is valid at 50 Hz and the second value is valid at 5000 Hz. At intermediate frequencies, a logarithmic interpolation is applied.

	t[m]	$\rho[\frac{\text{kg}}{\text{m}^3}]$	η [-]	ν [-]	$E[\frac{\text{N}}{\text{m}^2}]$
Finishing screed	0.05	1900	0.015	0.2	$17.4 \cdot 10^9$
Acoustic interlayer	0.008	25	0.3	0.2	$1.5 \cdot 10^5$ - $8.5 \cdot 10^4$
Thermal layer	0.05	125	0.1	0.2	$4.05 \cdot 10^7$ - $2.83 \cdot 10^7$
Concrete base floor	0.14	2445	0.015	0.2	$22 \cdot 10^9$

used on the test element and all hammer locations are accurately measured and listed in Table 6. At position 1, the tapping machine is positioned at the center of the test element and the hammers are aligned with the x-axis. At position 2, the tapping machine is placed such that the distance between the test element edge and the closest hammer is around 50 cm. In this position, the hammers are placed along the y-axis. Position 3 is located close to a corner of the test element, with the tapping machine placed at an angle of 45 $^\circ$ with respect to the x-axis. This tapping machine position is chosen to gain insight into the validity of assuming simply supported boundaries in mTMM.

The sound pressure level in the receiver room is measured with a sampling frequency of 48 kHz by means of a

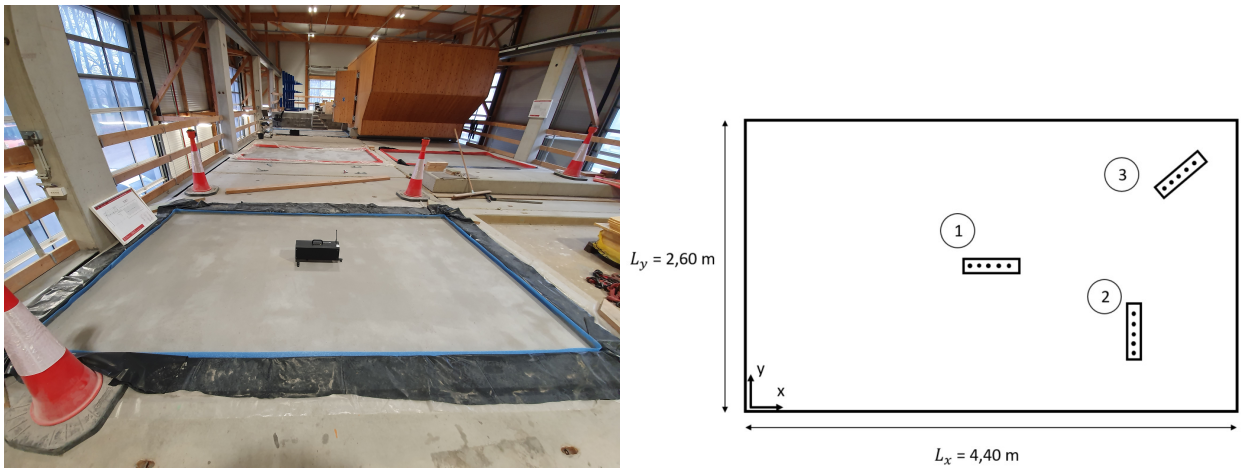

(a) (b)

Figure 8: Setup for the impact sound measurements: (a) laboratory setup, (b) schematic view of the tapping machine positions with respect to the test element.

Table 6: Tapping machine positions with respect to the test element, including exact hammer locations.

	Pos 1 [m]	Pos 2 [m]	Pos 3 [m]
Hammer 1	(2.03, 1.30)	(3.46, 0.53)	(3.97, 2.15)
Hammer 2	(2.13, 1.30)	(3.46, 0.63)	(4.04, 2.21)
Hammer 3	(2.23, 1.30)	(3.46, 0.73)	(4.12, 2.27)
Hammer 4	(2.33, 1.30)	(3.46, 0.83)	(4.19, 2.33)
Hammer 5	(2.43, 1.30)	(3.46, 0.93)	(4.27, 2.48)

sound level meter NTI XL2 using a manual scanning procedure (in accordance with ISO 16283-2:2020 [14]). The sound pressure level is measured at two different receiver locations for each tapping machine position. Averaging times are at least 30 s in accordance with ISO 10140-4:2021. The time history of the pressure signal is then transformed to the frequency domain using a Fast Fourier Transform (FFT) and subsequently converted into a sound pressure level. The total sound pressure level for a single tapping machine position is obtained by averaging the pressure over the two measurements.

From measurements performed on different layered floors (one without an acoustic interlayer and one without a thermal layer) it has become clear that the measured dynamic stiffness for both the thermal and acoustic layers are inadequate to accurately predict the measured impact sound pressure level. It has been shown that the obtained values from the measurement procedure to determine the dynamic stiffness, according to EN 29052-1:1993 [15], are not suitable for the prediction of sound insulation [16]. This can be attributed to several factors, including a dependence of the dynamic stiffness on the excitation force amplitude [16, 17] and a large variability of the dynamic stiffness values that has been shown by Round Robin testing [17]. To tackle this problem, the moduli of elasticity of both layers have been adjusted, since the dynamic stiffness itself is not explicitely used in the mTMM. The adjusted values are listed in Table 7. The low-frequent E of the thermal layer is decreased slightly such that the mass-spring-mass resonance frequency of a floor without an acoustic interlayer matches the measured decoupling frequency, whereas the high-frequent E is decreased such that the first thickness resonance frequency of the thermal layer better matches the measured thickness resonance frequency. Next, the low-frequent E of the acoustic interlayer is slightly increased such that the measured mass-spring-mass resonance frequency matches the measured decoupling frequency. Finally, the high-frequent E of the acoustic layer has been drastically increased because measurements on a layered floor with only an acoustic interlayer indicate that the acoustic interlayer behaves much stiffer than predicted in the original computations.

The measured and predicted sound pressure level in the receiver room as a result of three different tapping machine positions is illustrated in Fig. 9 in 1/48 octave bands. A difference larger than 20 dB is observed

Table 7: Optimized mechanical properties of each layer, used for accurate prediction of the sound pressure level. If a range of values is listed, the first value is valid at 50 Hz and the second value is valid at 5000 Hz. At intermediate frequencies, a logarithmic interpolation is applied.

	t[m]	$\rho[\frac{\text{kg}}{\text{m}^3}]$	η [-]	ν [-]	$E[\frac{\text{N}}{\text{m}^2}]$
Finishing screed	0.05	1900	0.015	0.2	$17.4 \cdot 10^9$
Acoustic interlayer	0.008	25	0.3	0.2	$4 \cdot 10^5$ - $4 \cdot 10^7$
Thermal layer	0.05	125	0.1	0.2	$2.5 \cdot 10^7$ - $3.5 \cdot 10^6$
Concrete base floor	0.14	2445	0.015	0.2	$22 \cdot 10^9$

between the predicted results at multiple frequencies of 10 Hz and 2 Hz, which is caused by the phase angle of the five hammers as discussed earlier. This phenomenon can also be observed in the measurement results, albeit with a smaller difference between the multiple frequencies of 10 Hz and 2 Hz. The first thickness resonance in the thermal layer causes a wide plateau in the measurement results, ranging from below 1000 Hz to well over 2000 Hz, whereas the predicted thickness resonance influences a smaller frequency region where it displays a peak value rather than a plateau. It can be concluded that the physical phenomenon of thickness resonances is included in the prediction method, but the predicted behavior differs from the measured physical behavior.

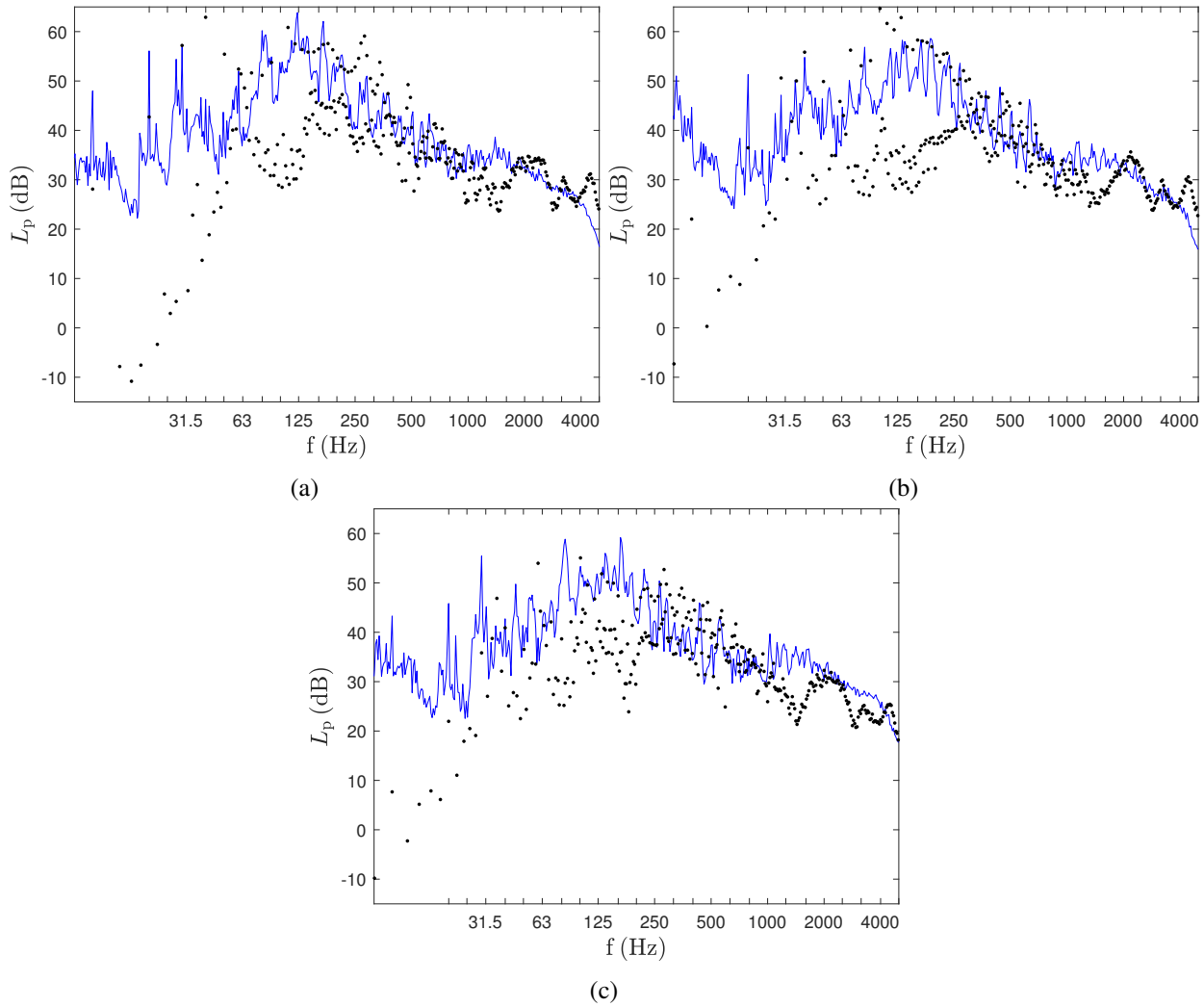

Figure 9: Sound pressure level in 1/48 octave bands for various tapping machine positions. Blue: measurement, black dots: mTMM with optimized moduli of elasticity. (a) Position 1, (b) position 2, (c) position 3.

The one-third octave band results for the three tapping machine positions are illustrated in Fig. 10. The same conclusion holds for the first two positions: the measured sound pressure level is predicted with good accuracy, using the optimized moduli of elasticity, until 800 - 1000 Hz, where the first thickness resonance of the thermal layer causes a difference between the measured and predicted results. However, the measurement and prediction results for tapping machine position 3 also deviate at low frequencies. This can be attributed to the assumed boundary conditions of the test element in the mTMM, which is very important for this particular tapping machine position, since it is located close to the corner of the test element. In reality, the full structure is simply supported and not the test element, leading to an underestimation of the sound pressure level in mTMM. Therefore, an equivalent mTMM model is constructed, which considers the horizontal dimensions of the full structure instead of just the test element. The mTMM requires a constant layer thickness, so an equivalent thickness is computed using a minimization of the error on the natural frequencies with respect to a FE model of the full structure, yielding an equivalent thickness of 22 cm. The equivalent mTMM model (cfr. Fig. 10) (c), yields significantly better predictions at low frequencies, i.e. frequencies up to 315 Hz. At high frequencies however, the sound pressure level in the receiver room is underestimated by the equivalent model, since in reality the test element dynamically decouples from the thicker floor.

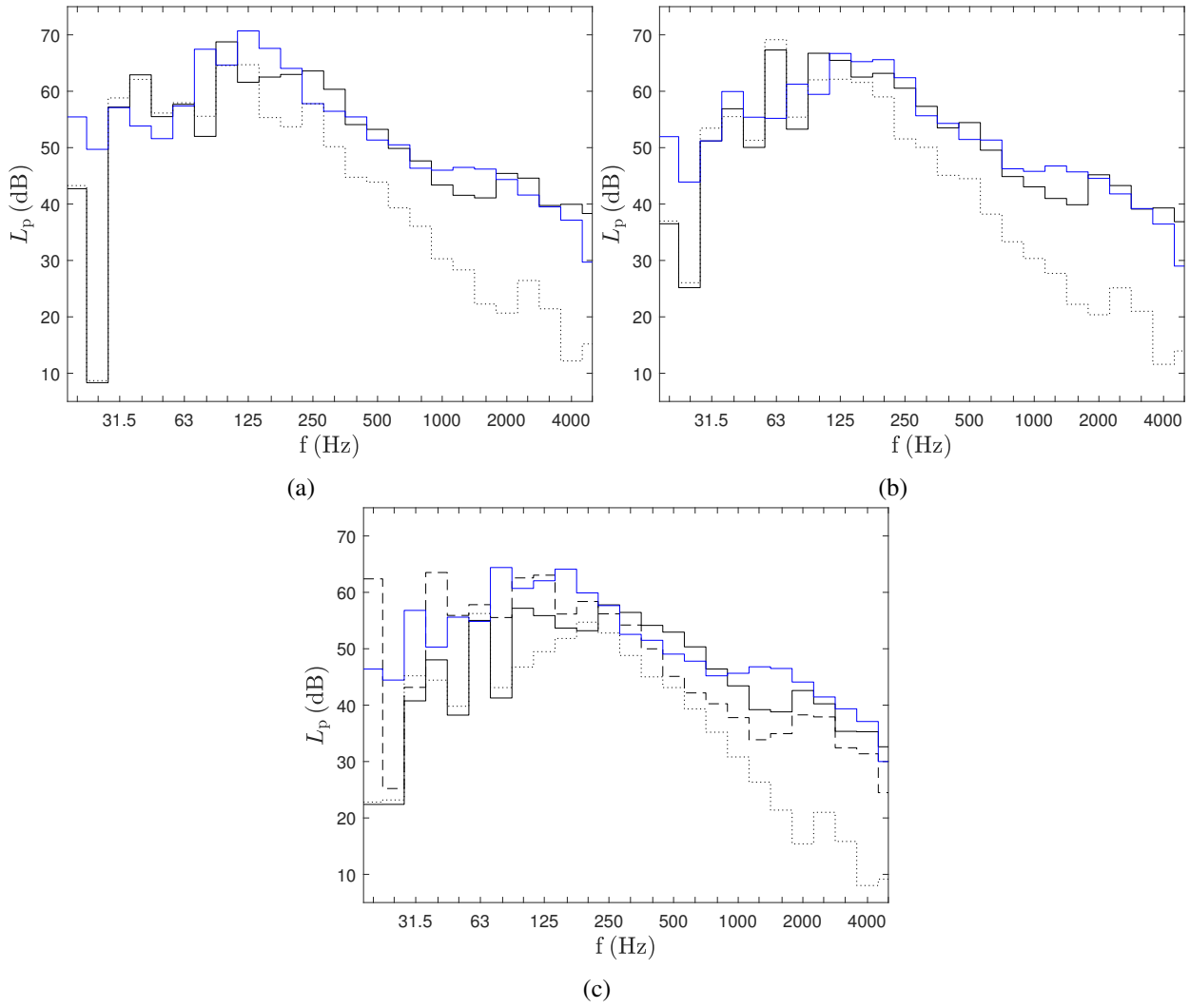

Figure 10: Sound pressure level in one-third octave bands for various tapping machine positions. Blue: measurement, black dotted line: forward mTMM prediction, black solid line: mTMM with adjusted moduli of elasticity, black dashed line: equivalent mTMM model. (a) Position 1, (b) position 2, (c) position 3.

6 Conclusions

Numerical validation has shown that mTMM predictions for the sound pressure level and the impact sound insulation improvement are very similar to a FE model of the test element. The computational efficiency of the mTMM is around 4270 times higher than the FE model for frequencies up to 2000 Hz. A second FE model has indicated the influence of adjoining concrete slabs, which are rigidly connected to the test element. The adjoining slabs have a large influence on the low-frequent modal behaviour and the additional mass leads to slightly lower predictions at high frequencies.

The uncertainty on the sound pressure level, resulting from tapping machine impacts on a floor, is highly dependent on the type of assessment. Varying the position of a single tapping machine can lead to a 95 % confidence interval with a width of 12 dBin the one-third octave band centered at 200 Hz, independent of the floor layering. On the other hand, taking the average over five tapping machine positions greatly reduces the 95 % confidence interval to about 3.7 dB. The relative difference between the analysis types is even larger when considering the uncertainty on impact sound insulation improvement at the one-third octave band centered at 200 Hz, wich amounts to a maximum of 5.8 dB for the single tapping machine position, while it is limited to 1.4 dB for the average over five tapping machine positions.

Narrow-band measurements of the sound pressure level in the receiver room for tapping machine impacts display a clear 2 Hz line spectrum. The difference between 2 Hz lines and 10 Hz lines starts around 20 dB at the lowest frequencies and decreases with increasing frequency. This effect is supported by mTMM predictions using a detailed source model, exhibiting the same pattern. It is shown that tapping machine positions close to the corner of a test element results in significant prediction errors in the mTMM if the floor surrounding the test element also contributes to sound radiation and invalidates the assumption of simply supported boundary conditions for the test element. In that case, the prediction accuracy can be improved by using an equivalent mTMM model which accounts for the size of the full structure instead of only the test element.

Acknowledgements

This research was funded by the European Research Council (ERC) Executive Agency, in the form of an ERC Starting Grant provided to Edwin Reynders under the Horizon 2020 framework program, project 714591 VirBAcous. The financial support from the European Commission is gratefully acknowledged.
The Belgian Building Research Institute have provided laboratory access to conduct experiments on different floor setups. The help of BBRI is gratefully acknowledged.

References

[1] V. Wittstock, "On the spectral shape of the sound generated by standard tapping machines," *Acta Acustica united with Acustica*, vol. 98, pp. 301–308, 2012.

[2] I. Vér, "Impact noise isolation of composite floors," *Journal of the Acoustical Society of America*, vol. 50, no. 4, pp. 1043–1050, 1971.

[3] J. Vastiau, C. Van hoorickx, and E. Reynders, "Numerical and experimental investigation of the narrow-band impact sound insulation of layered floors," in *Proceedings of the 51st International Congress and Exposition on Noise Control Engineering, Inter-Noise 2022*, Glasgow, United Kingdom, August 2022, paper accepted.

[4] J. Vastiau, C. Van hoorickx, and E. Reynders, "Wavenumber domain solution for impact sound prediction of finite floors with the (modal) transfer matrix method," in *Proceedings of the 50th International Congress and Exposition on Noise Control Engineering, Inter-Noise 2021*, T. Dare, S. Bolton, P. Davies, Y. Xue, and G. Ebbitt, Eds., Washington, D.C., August 2021, pp. 734–745.

[5] J. Vastiau, C. Van hoorickx, and E. Reynders, "A modal transfer matrix approach for the prediction of impact sound insulation," in *Proceedings of the 12th European Congress and Exposition on Noise Control Engineering, Euronoise 2021*. Madeira, Portugal: Sociedade Portuguesa de Acústica, October 2021, pp. 1745–1754.

[6] C. Decraene, A. Dijckmans, and E. Reynders, "Fast mean and variance computation of the diffuse sound transmission through finite-sized thick and layered wall and floor systems," *Journal of Sound and Vibration*, vol. 422, pp. 131–145, 2018.

[7] *ISO 10140-5: Acoustics – Laboratory measurement of sound insulation of building elements – Part 5: Requirements for test facilities and equipment*, International Organization for Standardization, 2010.

[8] N. Özkaya, D. Leger, D. Goldsheyder, and M. Nordin, *Impulse and momentum*. Springer, 2017, pp. 253–278.

[9] P. Wang, "Prediction with uncertainty quantification of the impact sound radiation from complex floors," Ph.D. dissertation, Department of Civil Engineering, KU Leuven, 2019.

[10] L. Cremer and M. Heckl, *Structure-borne sound: Structural vibrations and sound radiation at audio frequencies*, 2nd ed. Berlin: Springer, 1988.

[11] C. Crispin, D. Wuyts, and A. Dijckmans, "Thickness-resonance waves in underlays of floating screed," in *Proceedings of 50th International Congress and Exposition on Noise Control Engineering, Inter-Noise 2021*, Washington, D.C., August 2021.

[12] *ISO 10140-3: Acoustics – Laboratory measurement of sound insulation of building elements – Part 3: Measurement of impact sound insulation*, International Organization for Standardization, 2010.

[13] *ISO 12354-2:2017: Building Acoustics - Estimation of acoustic performance of buildings from the performance of elements - Part 2: Impact sound insulation between rooms*, International Organization for Standardization, 2017.

[14] *ISO 16283-2:2020: Acoustics - Field measurement of sound insulation in buildings and of building elements - Part 2: Impact sound insulation*, International Organization for Standardization, 2020.

[15] *EN 29052-1:1993: Acoustics: Determination of dynamic stiffness - Part 1: Materials used under floating floors in dwellings*, European Committee for Standardization, 1993.

[16] A. Schiavi, B. Pavoni, F. Russo, and M. Corallo, "Dynamic stiffness of resilient materials: some consideration on the proposed revision of iso 9052-1 standard," in *Proceedings of 20th International Congress on Acoustics*, 2010.

[17] C. Crispin, C. Mertens, and B. Ingelaere, "Estimation of the precision of the apparent dynamic stiffness measurement described in the standard EN 29052-1," in *Proceedings of Inter-Noise 2016, the 45th International Congress on Noise Control Engineering*, Hamburg, Germany, August 2016, pp. 6206–6217.